Reversible, all-perovskite SOFCs based on La,Sr gallates

Antonella Glisenti[a*] Andrea Bedon*[a] , Giovanni Carollo[a], Cristian Savaniu [b], and John Irvine [b]

a Department of Chemical Sciences, University of Padova, via F. Marzolo 1 – 35131 Padova, Italy

b School of Chemistry, University of St. Andrews, North Haugh, St. Andrews, Fife KY16, Scotland, UK.

Abstract

In this contribution, a reversible Solid Oxide Cell based on perovskites was developed. $La_{0.6}Sr_{0.4}Ga_{0.3}Fe_{0.7}O_3$ (LSGF) was chosen as electrode and deposited onto $La_{0.9}Sr_{0.1}Ga_{0.8}Mg_{0.2}O_3$ (LSGM) electrolyte. The cell was investigated from the morphological (SEM) and compatibility (XRD) point of view. Electrochemical investigation confirmed that the cell can operate in fuel cell and in electrolyser modes. Impregnation with CGO and Pd allowed a 15 times increment of the power density (until limit is the cell architecture). The same cell with an impregnated negative electrode was then tested in steam electrolysis mode in a non-reducing environment. The overall performance is slightly lower than state-of-the-art materials and comparable with similar perovskites, and in general is fair considering the needed cell optimisation (i.e a anode supported configuration is necessary). The cell (impregnated and not) activates at 0.7 V. Obtained data suggest thus LSGF/LSGM/LSGF cell, is promising as reversible SOC for intermediate temperature.

Keywords: Reversible Solid Oxide Fuel Cell, Symmetric SOFC, energy storage, perovskites, LSGF/LSGM, anode

1. Introduction

Solid Oxide Fuel Cells (SOFCs)[Mori 2020, Laguna Bercero 2012, Pryia 2020, Wunderlich 2016 1-4] are electrochemical devices very promising for sustainable conversion of energy. Among all the Solid Oxide Fuel Cells (SOFCs), a particular category deserves more attention for its novelty and the possible implications in current technology: the reversible cells. Reversible Solid Oxide Cells (ReSOCs)[Kazempoor 2014, Di Giorgio 2016 5-6] can convert H_2O and CO_2 into H_2, CO and O_2 when operating in electrolysis mode (by using, as an example, electrical energy from intermittent renewables) or convert chemical into electrical energy when operating in the fuel cell mode. These devices can, thus, operate as a secondary battery, so they can both store and produce electrical energy. This approach for energy storage and conversion was already demonstrated to be technologically and economically sustainable[7-12] and plants have been designed for optimizing roundtrip efficiency.[13] Several researchers developed fuel cell systems that address multiple market segments that include renewable H_2 production, power to gas, energy storage, grid balancing, and fuel flexible distributed power generation from a single core high temperature reversible SOFC unit.[14-17]; reversible systems are also theoretically investigated to evaluate the requirements for higher efficiency and lower C-poisoning. [18-20] Reversibility can contribute to decrease the impact of sulphur poisoning at the anode when using fuels different than hydrogen; it was observed, in fact, that SO_2 adsorption in SOFC is reversible; attention has to be spent when Sr is present because of the irreversible formation of $SrSO_4$. [21]. A particularly interesting version of the ReSOCs are the symmetrical SOCs (Sy-SOCs). In this device the same material is used both for anode and cathode. With symmetrical configuration the production of SOCs can be simplified (only one thermal step) and compatibility problems are minimized.[22, 23] The material requirements become more severe in Sy-SOCs the electrode being required to be stable and electrocatalytically active both under oxidizing and reducing condition.[23] Focusing on materials, reversibility has been demonstrated on Yttria Stabilized Zirconia (YSZ) based SOC and, moreover, several configurations have been hypothesized for Sy-SOCs.[24-25] In both cases, however, high temperatures (> 800°C) are required to reach good performance. It has also to be considered the need to avoid the use of Nickel whenever the SOFC fuel is C-containing.

The cell developed in this contribution is not strictly symmetrical. However, it was designed under the same principles of homogeneity that drive symmetrical cells: two equal electrodes have been added at both sides of an electrolyte. Then, only one was impregnated, because the other one already owned a sufficient activity for its role. It would have been simple to keep the cell exactly symmetrical, by impregnating also the other electrode, but it would have been unnecessary. The idea behind symmetrical cells is to keep fabrication as simple as possible, and this principle prevailed on the strict adherence to the symmetricity. Anyway, it has been decided to still define the cell "symmetrical", because in fact no separated treatment for anode and cathode is necessary. The cell is Ni-free operating at temperature $\leq$ 800°C, and based on the use of $La_{0.6}Sr_{0.4}Ga_{0.3}Fe_{0.7}O_3$ (hereafter LSGF) as electrode and $La_{0.9}Sr_{0.1}Ga_{0.8}Mg_{0.2}O_3$ (LSGM) as electrolyte. Such La, Sr, Ga based perovskites provide a formidable framework for the design of a symmetrical, reversible cell with remarkable homogeneity.

As it is described in previous works, LSGF has been successfully tested as a suitable platform with high stability for custom functionalisation, and it was able to develop decent electrode activity.[26] The tests shown here extend its application to the whole category of the solid oxide cells, also including electrolysers, so that a fully reversible cell made with LSGF electrodes can be fabricated. To the best of our knowledge, it is the first time LSGF is used to prepare a SOEC electrode, similar materials (for example LSF) have already been tested with promising results;[27] gallium is expected to increase stability and durability. The aim of this series of experiments is to test the feasibility and the performances of a LSGX based symmetrical reversible cell for energy storage, with X being Mg for the electrolyte and Fe for the electrodes. LSGM is a consolidated electrolyte material;[28,29] it shows good conductivities at intermediate temperatures, and recently has been tested also for SOECs.[30,31] Unfortunately, LSGM was proven to be not fully compatible with some other common materials for SOECs, as Ni, ceria [32] and cobalt containing perovskites.[33] In fact, degradation of components is a major issue for SOECs, that found their industrial application to be limited by a fast loss of performances due to a variety of reasons, including: formation of insulating phases at the interfaces, physical degradation of the electrodes/electrolytes, migration of impurities across the components.[34] Hence, in order to reach the economical sustainability of these devices, the primary focus is on stability, rather than cell power, hoping to provide a stable backbone for cells, whose performance can be enhanced by proper coupling with other phases. The very similar composition of the two LSGF and LSGM should avoid the formation of any insulating phases with long term depleting effects, and in any case the elimination of nickel from the anode makes impossible the appearance of the insulating $LaNiO_3$, which affects the LSGM/Ni interfaces.
In this contribution, the compatibility between LSGF and LSGM has been verified by means of an appropriate XRD test. The first fuel cell tests were conducted on a cell with both the electrodes made of pure LSGF. Then, a second cell was prepared, in an attempt to improve performances, trying to solve the most severe issues that affected the first tested cell with an impregnation of the negative electrode with CGO and Pd. The impregnation with CGO and Pd has been chosen on the basis of literature, as it seemed suitable for the kind of electrocatalytic activity that was required.[35] The so-obtained cell was then tested in fuel cell operation, and performances have been compared with the simple non-impregnated cell. Impedance spectroscopy and polarization curves were collected during the cell operation, impedance data were fitted on an appropriate equivalent circuit to determine the cell Area Specific Resistance (ASR). Both the electrodes, LSGF and LSGF impregnated with CGO/Pd, have been examined by means of Scanning Electron Microscopy (SEM), to identify the structures formed during the impregnation. SEM, along with XRD, has also been employed on a tested cell to find the cause of a performance decrease of non-impregnated LSGF anode above 800 °C. Following the good performance of the Pd/CGO impregnated electrode, the same device was tested as an electrolyser for steam electrolysis, and also in this case EIS data and polarization curves were collected. At the end of this work, it was possible to obtain a fair indication about how LSGF can behave in a reversible SOFC.

2. Experimental

2.1 Cell preparation

The cells studied in this work are supported on thick electrolyte, prepared by pressing a LSGM powder (commercial LSGM9182, Kceracell, Korea) into pellets and then firing them at 1400 °C for 6 hours: thickness of the pellet is around 1.2 mm with a 2 cm diameter. The LSGF powder used for electrodes was synthesized via a solid-combustion route, with the same procedure explained in a previous work.[36] Two different inks were prepared for the screen printing of the electrodes on LSGM: a composite LSGF 50%/LSGM 50% and a pure LSGF ink. Ink preparation involved grinding of the powders and mixing them with proper amounts of α-terpineol and polyvinyl butyral binder, PVB. Cells were fabricated by screen printing two layers on both sides of the electrolyte, first layer is LSGF/LSGM composite to improve electrolyte/electrode contact and second is pure LSGF, the mask used for printing is a circle of area 1.11 cm^2. Cells were then fired at 1100 °C. A second type of cell differs at the negative electrode side: in fact, LSGF underwent an impregnation with CGO (mixed oxide of Ce 90 at% and Gd 10 at %) and Pd. In this case, LSGF provides ionic and electronic conductivity, mechanical support and stable contact with the electrolyte. For the impregnation some drops of a solution of $Ce(NO_3)_3$, $Gd(NO_3)_3$ and DTAB (1-hexadecyl trimethyl ammonium bromide, 1wt%) were dropped on the electrode until it wetted the whole surface, the cell was then treated at 750 °C for 30 minutes. This procedure was repeated until the electrode gained 10-15 wt% extra mass compared to its weight. After the CGO deposition, a single drop (around 10 µl) of $[Pd(NH_3)_4](NO_3)$ solution was used to impregnate palladium, then, another treatment at 750 °C for 30 minutes followed. This procedure was repeated until a Pd content of about 1wt% was reached. Finally, a gold grid was painted (using a gold paste) on both the electrodes and the cell was further treated at 750 °C for 30 minutes.

2.2 SEM and XRD measurements

SEM images of the electrodes have been taken, using a Jeol JSM-6700F Scanning Electron Microscope equipped with field emission gun electron source. Samples have been gold sputtered prior to the analysis to increase conductivity.

Compatibility test between LSGF and LSGM consisted in finely grinding the two powders in a mortar (50/50 weight ratio) and in treating them at 1100 °C for 8 hours. XRD analysis has been then performed using a PANalytical Empyrean machine, equipped with a Cu X-ray tube and a primary beam monochromator (CuKα1).

2.3 Electrochemical measurements

Fuel cell measurements were performed sealing the cell on an alumina tube with a specific ceramic paste (Aremco Ceramabond 552 VFG). The electrodes impedance measurements and polarization curves were collected with a Solartron Frequency Response Analyser/Electrochemical Interface (1287/1255 for fuel cell testing and 1252/1470 for electrolysis). In fuel cell measurements, negative electrodes could be fed with 5% H_2 in N_2 or pure H_2 fuel mixtures. Fuel could either be directly sent to the cell (dry) or made passing through a bubbler containing water (wet); in these experiments wet 5% H_2, dry 5% H_2 and wet 100% H_2 fuel mixtures were used at a flow rate of 50 ml/min. Air was fed to the cathode at 100 ml/min. During electrolyser measurements, negative electrode was fed with steam in N_2 with concentrations 5% (500 ml/min) and 10% (250 ml/min); these flows are the minimum necessary to enough steam to guarantee a good sweeping of the electrode surface.

3. Results and discussion

First of all, the used materials underwent a compatibility test. Then, the cells with the tested materials have been fabricated and tested.

3.1 Compatibility

Results of the compatibility tests are shown in **Errore. L'origine riferimento non è stata trovata.**. LSGF and LSGM are similar perovskites and all the reflections overlap, so it is difficult to notice structural modifications because the direct reaction between them would produce a phase with the same reflections. All the reflections of the perovskites are observed, as well as a number of minor peaks relative to a $LaSrGa_3O_7$ phase that was already present in the LSGF powder. The intensity of $LaSrGa_3O_7$ peaks after the treatment at 1100 °C for 8 hours in the compatibility test is half the one it has in simple LSGF: this result is consistent with the hypothesis that it only originates from LSGF powder (LSGF and LSGM were mixed in equal amounts). The $LaSrGa_3O_7$ phase is a common product of the degradation of LSGM due to migration of atoms through the electrode/electrolyte interface [37,38] and it is of particular relevance that, in the present system, no increase in the abundance of this phase is observed, other than the amount already present in LSGF powder. Its presence had already been investigated in a previous work, and its concentration has been found not to be modified by different thermal treatments suggesting that it is not a sign of material degradation. [36] Its appearance could be avoided lowering Ga concentration in LSGF (appearance of Ga rich phases are far less common if Ga stoichiometric coefficient is 0.3) at the expense of a part of performance,[39] however, since it does not cause any harm to the main phase, it has been preferred to tolerate its presence to obtain higher overall conductivity. There is also a small signal related to $LaSrGaO_4$, that again was already present in pristine LSGF. No new extra peaks appear.

The main difference between XRD patterns of LSGM and LSGF is the splitting of some LSGF peaks, due to the rhombohedral distortion. The splitting is observed also after the thermal treatment as evidenced for the peak at 68° in upper-right corner of Figure 1. The change in relative intensities of the two components is probably caused by the underlying LSGM reflection: it is closer to the lower-angle component of the LSGF doublet, so it unbalances the ratio between the two components in favour of the lower-angle one. The permanence of the splitting after the treatment excludes major breakdown of LSGF phase, but minor modifications cannot be excluded as they would result in reflections overlapping pristine phases' ones.

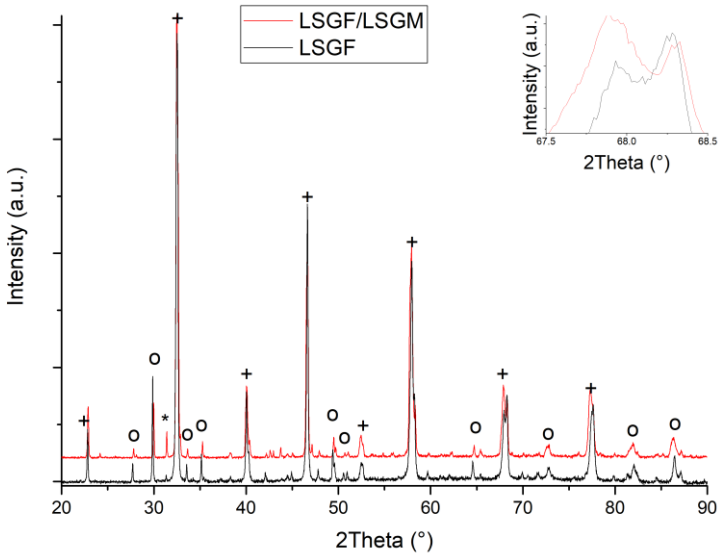

Figure 1 XRD pattern of calcined LSGF and LSGM powders, compared to pristine LSGF. + signs mark perovskite peaks, that are in common between LSGF and LSGM. O signs mark $LsSrGa_3O_7$ peaks, and * marks the $LaSrGaO_4$ peak.

3.2 SOFC test on LSGF based cells

The polarization curves of the pure LSGF based cells are shown in Figure 2; the OCV, close to 0.9V for 5% H_2 (average/low value), increases to 1.05 V with pure hydrogen as a fuel. This confirms the possibility to realise an LSGF-based symmetrical cells.

Figure 3 shows impedance curves with different fuels and reveals that electrode resistances are very high; at the same time ohmic resistance is around 2-3 $\Omega \cdot cm^2$, which can be considered a fair value given the thickness of the electrolyte. [40,41]

The CPE in parallel with a resistance accounts for the processes at the electrode. In addition, a Warburg element has been included because of some diffusion-limited processes already observed in this class of materials.[42]

The large variations in polarisation resistance depending on fuel suggest that the limiting process can be anode (negative pole) controlled, consistently, the LSGF cathode tends to show far lower resistances (around 3 $\Omega \cdot cm^2$). Electrodes' resistance (sum of Warburg resistance and polarization resistance) is reported in Figure 4, with the equivalent circuit used for fitting.

3.2.1 Effect of H_2 concentration

In the case of a pure LSGF anode, we observe a very high electrode resistance (see Figure 3 and Figure 4, ASR (Area Specific Resistance) of common anodes is around 10^{-1} $\Omega \cdot cm^2$), and power output is very low, as shown in Figure 2. Among all the mixtures, the feeding with wet 5% H_2 gives the best results. Consistently, the performance improvement observed with only 5% of hydrogen is symptomatic of a preference of the material for less reducing environments due to stability issues.

Only in the case of the LSGF symmetrical cell the Warburg element has proven to be redundant, as a simplified Randles circuit (same circuit as shown but without Warburg element) is able to satisfyingly fit the curve. This means that there is only one limiting step, which consists in the polarization of one electrode. This process is very strongly dependent on hydrogen concentration, and behaves more efficiently if a lower hydrogen concentration is used. Some assumptions can be deduced from this. The limiting electrode is the anode (thus such a great effect of fuel), and the limiting process is surely influenced by hydrogen (given the high ASR variations depending on its concentration in the mixture).

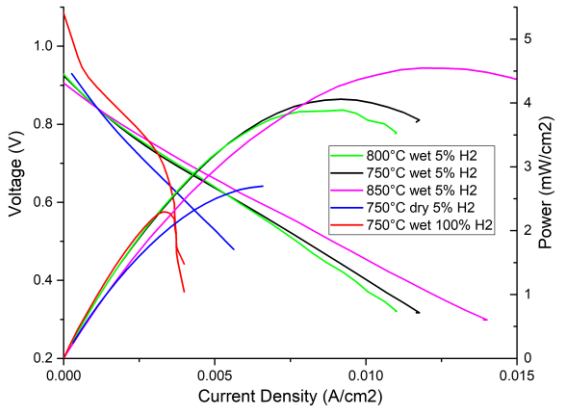

Figure 2 Polarization curves and power of symmetrical pure LSGF cells.

Hydrogen oxidation on perovskite anodes is radically different from the corresponding reaction on Ni cermets, as the phase which provides hydrogen adsorption, electrons and oxygen ions is the same and therefore there is no Triple Phase Boundary.

A possible explanations can be found in a work by Zhu et al. [43]. This work has analysed the impedance response of iron-based perovskite anodes under hydrogen, and concluded that the main limiting process is hydrogen dissociative adsorption. Fu et al. reached the same conclusion for (La,Sr)(Ti,Mn)O_3 perovskites.[44] The decreased performance of the cell with pure H_2 feeding is due to a very low limiting current, well indicated by the sudden decrease of the i/V curve and corresponding to 0.0037 A/cm^2.

Following Zhu's model, such a limitation could be ascribed to a very low oxygen coverage of the surface that limits available sites for hydrogen adsorption. The small increase of current at voltage under 0.5 V was described in the same paper as a change in surface oxygen coverage induced by the decreasing potential and is in accordance with this interpretation. At lower pH_2 (hydrogen partial pressure), a better oxygen coverage removes the strict limit observed with pure hydrogen, this implies a very high dependence of oxygen superficial sites concentration on pH_2 for LSGF

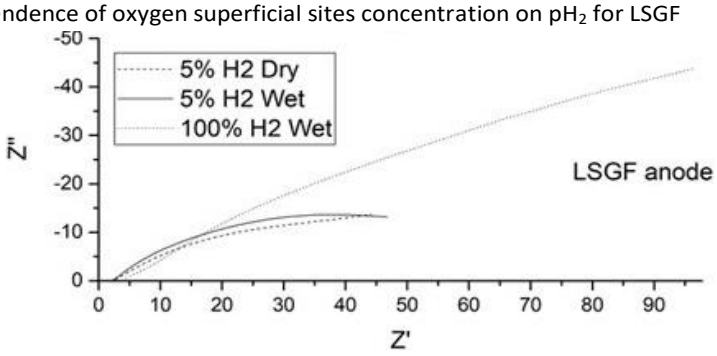

Figure 3 Nyquist plots of impedance spectra of cells with LSGF anode, with different fuels at 750 °C. Electrolyte is LSGM and cathode LSGF.

3.2.2 Effect of temperature and cell degradation

Contrary to expectations, at 800 °C polarization resistance is higher than at 750 °C, and consequently also power output decreases. This could be caused by the electrode degradation (LSGF starts to degrade in reducing atmospheres at temperatures higher than 800 °C, as it determined in previous investigations)[36], but probably this is not the primary cause of the performance decrease. Indeed, at 850 °C, under conditions that should degrade LSGF more rapidly, power increases again, and the resistance decreases. This degradation appears irreversible, as cooling at 750 °C does not allow full recovery of the performances previously observed. A second heating over 750 °C causes another loss of performances, thus it seems it is not a simple thermal induced degradation (which would increasingly jeopardise performances at higher temperature): instead, it is heating passing over this temperature threshold that damages the cell.

A visual analysis of the electrode after the measurements evidences an apparent melting of the painted gold collector, indeed, the surface of the electrode seemed covered by some kind of goldish glaze. The anode condition was deeply examined by means of SEM (Figure 7). Image B, compared to the electrode before the measurements (image A) evidences a more compact structure and a variety of new features formed on the material, probably following the LSGF deterioration expected at these high temperatures. The surface of the electrode appears covered by a thick layer coming from gold collector, in some areas (images C and D) it is still possible to observe the LSGF particles below the newly formed covering, and to appreciate the crystallization of gold that followed cooling. A molten gold layer above the electrode surface can block porosities and prevent LSGF contact with gases.

If the melting happened between 750 °C and 800 °C, it could explain the performance decrease observed between these temperatures: each time gold melts it further degrades the cell by loss of contact and further increase of temperature would improve performances of the gold non-passivated surface, as it is observed. Nonetheless, gold normally melts over 1050 °C, so an intervention of LSGF in promoting gold melting has to be considered. Further tests revealed no such effect if LSGF on CGO is simply treated at 800 °C-850 °C under 5% H_2 atmosphere, without being part of a fuel cell. So, either polarization is needed or the effect is caused by local temperature increase at the surface due to the exothermicity of the reactions. At the same time, nothing similar happened on the cathode side, so probably LSGF manifests this effect only under reducing atmospheres. The XRD pattern of the electrode (Figure S1 – Supporting Information) is not helpful in explaining the situation, it shows a great amount of gold and that perovskite is still present; in addition, the formation of a large number of oxides, resulting in all the minor peaks of the pattern, is observed. Regrettably, the crowding of minor reflections makes impossible to identify the oxide phases with precision. In any case, gold alloys or formation of any compound with gold is excluded, and some degradation of the LSGF is confirmed.

Therefore, above 750 °C two distinct degradation processes are identified: a gold melting over active electrode surface and chemical electrode LSGF degradation due to the reduction of the cations of the perovskite. The gold melting causes a sudden depletion of the power output and has been clearly observed, but can be avoided in future test simply adopting a different current collector; the LSGF degradation produces a progressive loss of performances on the medium term.

3.3 SOFC tests on impregnated cells

For impregnated cells, SEM was used to verify the formation of the nanoparticles after impregnation. Then, the cells were electrochemically tested.

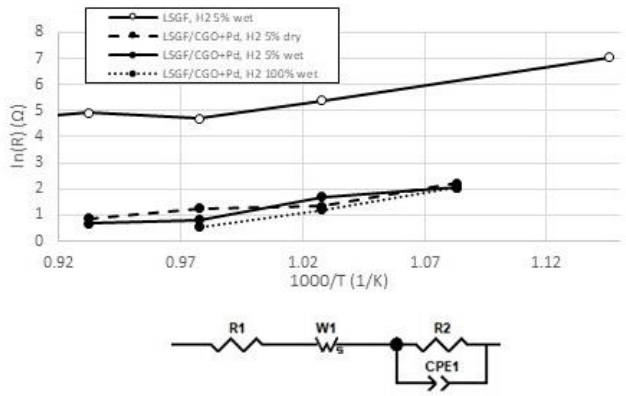

Figure 4 Above: Electrode resistance (Ω·cm^2) of the samples as calculated from EIS. Anode is indicated in legend, electrolyte is LSGM, cathode is LSGF. Below: equivalent circuit used for ASR calculation from EIS data.

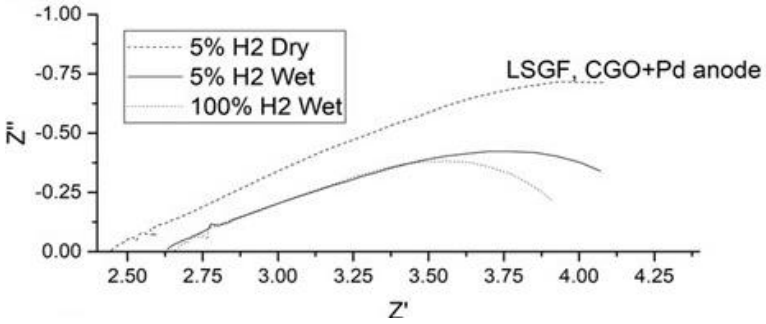

Figure 5 Nyquist plots of impedance spectra of cells with LSGF impregnated CGO/Pd (above), with different fuels at 750 °C. Electrolyte is LSGM and cathode LSGF.

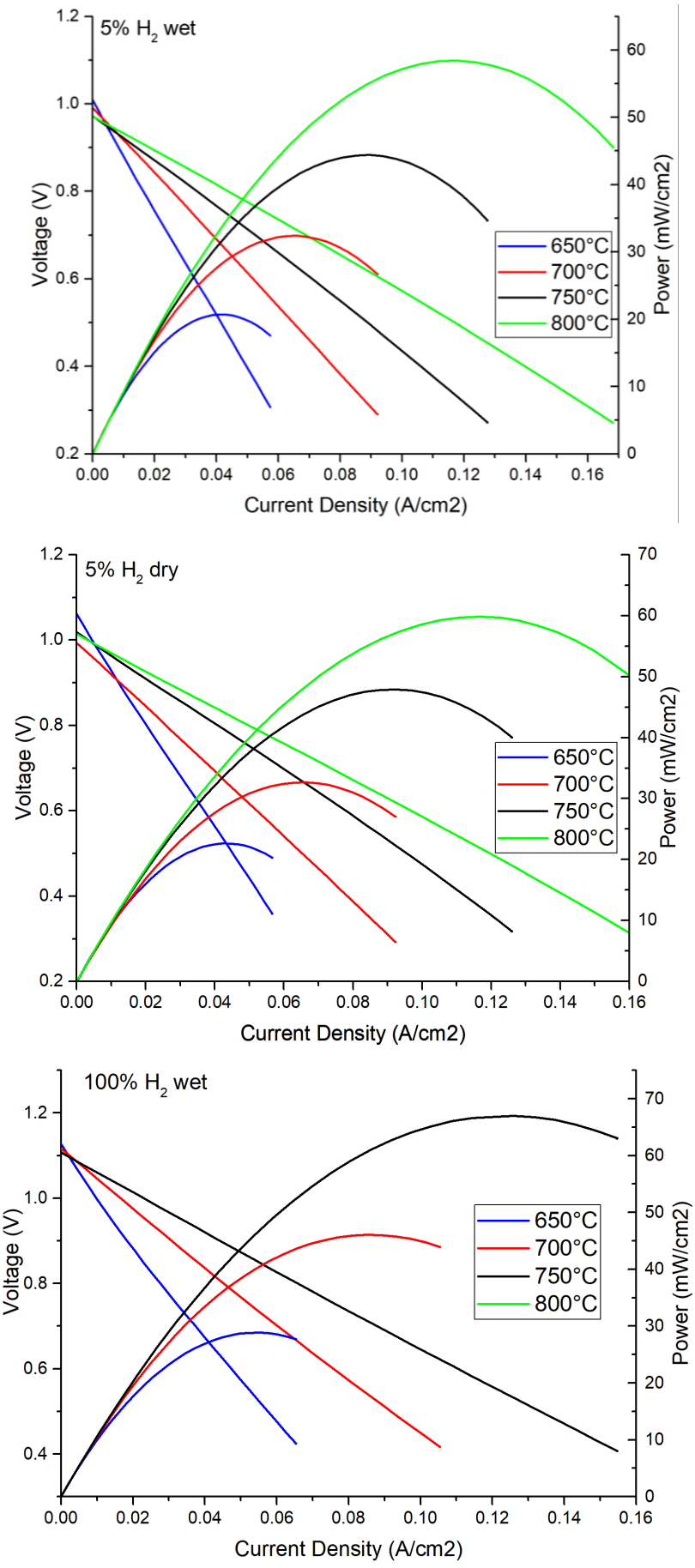

Figure 6 Polarization curves and power of fuel cell with Pd/CGO impregnated anode with different fuels.

3.3.1 SEM images

The good coverage of the impregnated electrode is easily visible in SEM images (Figure 7 E): CGO coated all the surface of the LSGF particles forming a smooth layer above them. In Figure 7 F it is possible also to observe the active palladium nanoparticles and to measure their size, that is around few tens of nanometres. The palladium dispersion is optimal, as well as its stabilization by the CGO substrate.

3.3.2 Electrochemical performance

The impregnation of the anode (negative pole) with CGO/Pd decreases the electrode resistance of more than one order of magnitude (Figure 4 and Figure 5) and greatly improves the performance of the cell (Figure 6). Palladium provides an excellent catalytic activity for fuel oxidation reaction, and the extreme improvement it induces, confirms that the poor electrocatalytic performance at the anode was responsible for the low power output of the pure LSGF cell. The influence of the hydrogen partial pressure and presence of water appears almost negligible from the impedance measurements at open circuit that are summarized in Figure 4. Variations in hydrogen concentration do not affect performances at the same extent noticed for the non-impregnated cell, but there is some dependency of the ASRs from the fuel used, so anode could be still involved. The Nyquist plot (Figure 5) shows an asymmetric loop, a shape different from the LSGF/LSGM/LSGF cell, and the ASR is reduced as well. The shape of curve in Nyquist resembles what had been previously observed for LSGF cathodes in terms of both shape and resistance magnitude, that was associated to oxygen dissociative adsorption and diffusion processes. [26] Ohmic resistance is comparable to the pure LSGF cell: the impregnation did not affect the electrolyte or the LSGF/electrolyte interface so no variation was expected.

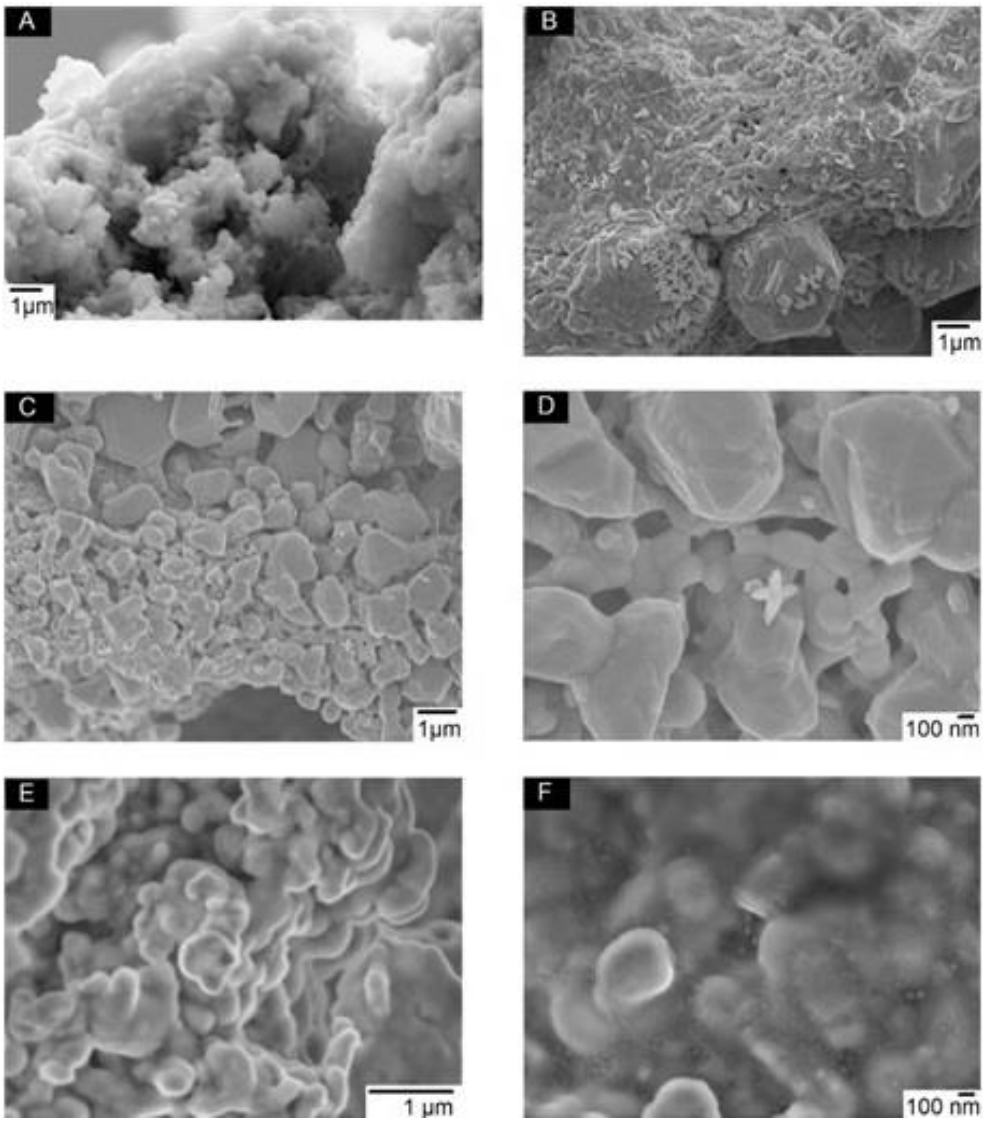

Figure 7 SEM images of tested cells. A: cross section of a LSGF electrode. B: cross section of LSGF anode after test as fuel cell. C and D: surface of LSGF anode after test as fuel cell. E and F: surface of a LSGF electrode impregnated with CGO/Pd.

The fitting of these curve indicates both a limited diffusion (represented by the Warburg element) and a polarization resistance (represented by the R//CPE) concur in limiting the process, but at 750 °C and 800 °C the only Warburg element is

significant. A comparison between Bode plots of phase of the two cells (with and without CGO/Pd in the anode – see Figure S2 – Supporting Information) confirms that the limiting process for the pure LSGF and the impregnated cells are radically different: apart from the different magnitude, the apex frequency has shifted by a factor 10^{-2}, reaching the same values observed for LSGF cathodes. Altogether, this means that now the main limiting process is the ionic conduction of LSGF, probably at both electrodes: ASR is similar to cathodic contribution measured for a LSGF electrode, and the R//CPE (that models a polarizable electrode through a resistance in parallel with a CPE) has analogous behaviour, but the variations depending on fuel require also the participation of the anode. With pure hydrogen the resistance is lower, as observed in Figure 6 (the vacancies of anodic LSGF are expected to be present in higher concentration). The lower contribution of the polarisation process represented by the R//CPE element in the impregnated LSGF cell is probably to the duplication of the resistance related to bulk diffusion: bulk diffusion is limiting in both the electrodes, but the polarization process is relevant only at the cathode. Thus, ionic diffusion in LSGF appears in impedance spectra twice (one time for each electrode) and becomes preponderant compared to other processes. The complete disappearance of the contribution due to hydrogen dissociative adsorption confirms LSGF is not involved in this process, which is carried out by impregnated palladium, and that now anodic resistance is negligible compared to the cathodic one.

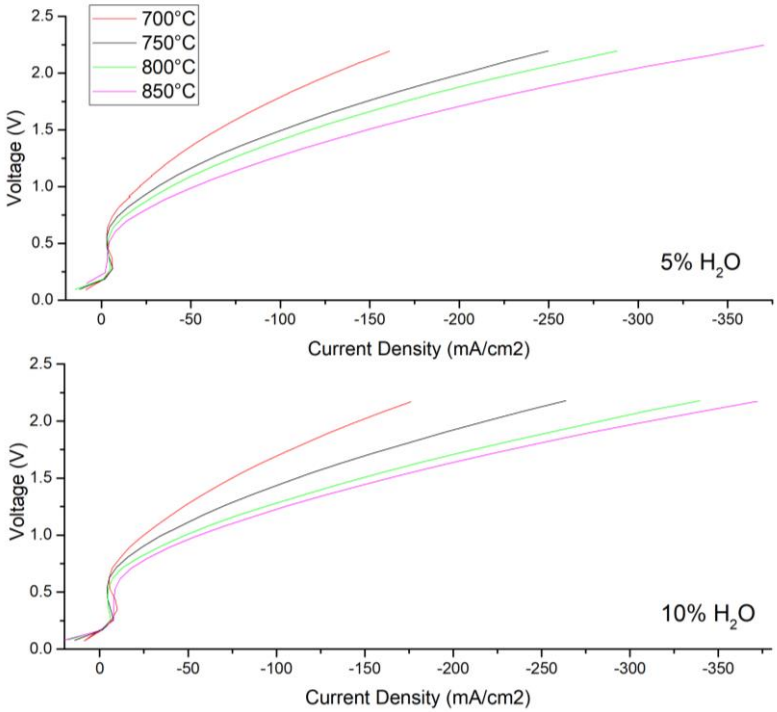

Figure 8 Polarization curves of cell with impregnated negative electrode as electrolyser at different temperatures. Electrode is fed with 5% steam in N_2 (above) and 10% steam in N_2 (below).

A posteriori, the initial assumption to consider only one electrode during fitting with model circuit has proven to be correct: non-impregnated cell is anode limited, while impregnated cell is limited by the same process happening at both electrodes, that is modelled by only one Warburg element. The cell power output reaches 60-70 $mWcm^{-2}$, with only little dependence on the hydrogen partial pressure (Figure 5). The OCV is very good, being extremely close to the thermodynamic potential in particular with pure H_2 feeding, this suggests the cell probably could be able to reach good efficiencies.

Interestingly, the detrimental effects of heating over 750 °C observed with the pure-LSGF cells does not affect this cell: it seems that CGO was able to coat and to prevent contact between LSGF and gold, and this could be a further confirmation that the problem arose due to the interaction between these two phases. CGO prevents also an extensive contact between LSGF and hydrogen fuel potentially allowing operation at temperatures higher than 750 °C, but it is not clear at this point if CGO effectively passivates all the LSGF surface. It must also be underlined that the influence of the atmosphere does not necessarily mean that LSGF is exposed, as there is an equilibrium between LSGF and CGO, if the latter is reduced it could drain LSGF's oxygen as well. However, if the passivation is not completely effective, some contact between LSGF and hydrogen happens and the certain outcome is a medium/long term degradation of the electrode. To precisely assess this matter, appropriate stability test will be performed.
On the basis of the reported results, a precautionary temperature of 750 °C must be considered as the maximum allowed; this limit, in any case, is well above the safe temperature to avoid gallium evaporation from LSGM, so anode stability should

not be an issue. It becomes gradually clearer that the materials under examination are promising, but must be employed only for Intermediate Temperature operation and should be never heated over 700 °C, at least when in fuel cell mode.

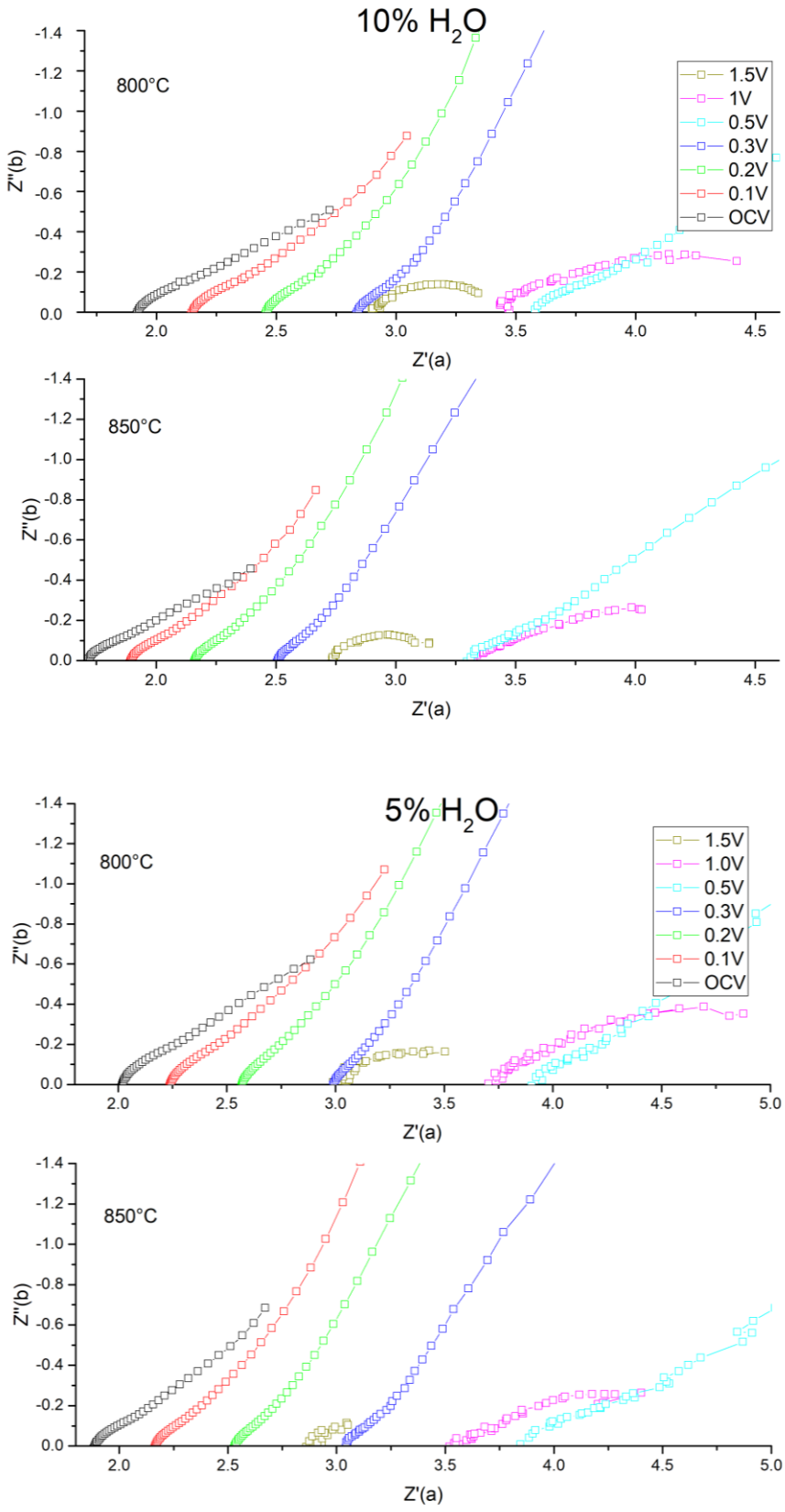

Figure 9 Impedances in electrolysis mode at 800 °C and 850 °C with 5% and 10% steam.

3.3 Solid Oxide Electrolysis Cell test

Polarization curves of the CGO/Pd impregnated cell in electrolysis mode are shown in Figure 8; they have in general an "S" shape and maintain it throughout the sampled temperature range. Overall performance is slightly lower than state of the art materials and comparable with similar materials,[45] and in general is fair considering the thick electrolyte employed and that no reducing atmosphere was used. Curves begin at OCV with a very steep slope that continuously increases until 0.5 V even reversing curve direction (between 0.3 V and 0.5 V an increase of voltage corresponds to a decrease of the measured current). Then, over 0.7 V slope changes abruptly towards a higher production of current; temperature seems to have no influence on this onset potential. No other transition is observed in the sampled interval.

Impedance spectra (Figure 9) show large polarisation resistances at potentials close to OCV, then they suddenly decrease between 0.5 V and 1 V, the same voltage that induces polarization curves' slope change. Polarization resistance at 800 °C is around 2.5 $\Omega \cdot cm^2$ with 1.0 V and 0.6 $\Omega \cdot cm^2$ with 1.5 V, and at 850 °C is around 2 $\Omega \cdot cm^2$ with 1.0 V and 0.4 $\Omega \cdot cm^2$ with 1.5 V. There is only little variation between 5% or 10% H_2O feeding. Ohmic resistance trend is interesting: at OCV is at its lowest, and it increases with increasing voltage until 0.5 V. A further increase in potential also decreases ohmic resistance, although the variation has not the same magnitude of the polarization resistance's one.

The cell activates only at a potential higher than 0.7 V, the decrease of resistance (polarization and ohmic) and the increase of current suggest a chemical transition in the material necessary to activate the process.[46] Conversely, up to 0.7 V some highly resistive phenomenon prevents an efficient electrolysis of steam. Figure 10 shows a comparison between a polarization curve of a cell as the one previously described and a second electrolyser with a pure-LSGF cathode at 600 °C. Apart from poor activity of the cell without impregnation, it is relevant that the activation happens at the same potential. This is even more evident looking at the second derivatives of the I vs V curves: they both cross zero at 0.7 V, and this means that the change of the activation of the electrolysis process (change of slope) happens at the very same point. The second derivative, shown in the same Figure 10, is added to clarify that activation begins at 0.7 V, although proceeds at different speeds after that point. This confirms that activation is not temperature dependent, and that impregnated CGO/Pd is not involved. At the cathode (negative pole), LSGF has only a secondary role, providing mechanical support and connection between the electrolyte and the active phase, so probably the cause of the high resistance at potentials close to OCV could be related to some phenomenon happening at the anode (positive pole), although more investigation is needed to assess it.

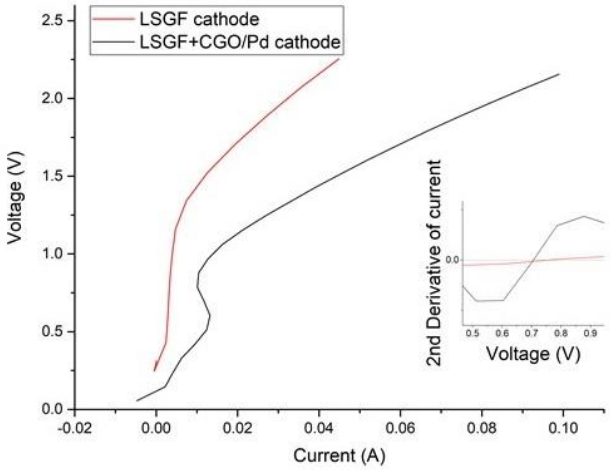

Figure 10 Comparison between polarization curves at 600 °C of electrolysers with anode LSGF, electrolyte LSGM and cathode as indicated in legend, cathode is fed with 50% H_2O in N_2 and anode is fed with air.

Conclusions

In this work a symmetrical all-perovskite solid oxide fuel cell has successfully developed. The cell has been obtained by using LSGF ($La_{0.6}Sr_{0.4}Ga_{0.3}Fe_{0.7}O_3$) as electrode and LSGM ($La_{0.9}Sr_{0.1}Ga_{0.8}Mg_{0.2}O_3$) for the electrolyte and was tested both in fuel cell and electrolyser modes.

Some critical flaw has been detected at the anodic compartment of the SOFC; in particular, a very high anodic polarization resistance led to a low power output. In addition, LSGF in reducing environment promoted gold contacts melting hence covering its own active surface; this curious effect compromises the anode in a short time, and probably deserves more attention as, to our knowledge, it has never been reported before.

In order to enhance electrocatalytic activity and to avoid contact between LSGF and gold, the anode was impregnated with CGO and nanoparticles of Pd, and this allowed to reach both the prefixed goals. SEM confirmed the good dispersion of infiltrated particles. Notably, after impregnation power density with anode impregnation was improved from 4 mW/cm^2 to

60 mW/cm^2, limited this time mainly by cathode performance. The CGO layer was able to avoid contact between LSGF and gold hence preventing gold melting, but it is unclear if it is able to passivate LSGF towards reduction in the long term.
The same cell with an impregnated negative electrode was tested as steam electrolyser in a non-reducing environment and promising performances were observed. A high resistance mechanism was found to prevent electrolyser operation under 0.7 V, this is independent on temperature, Pd/CGO presence and cathodic gas composition. More investigation is required to precisely assess the cause of this resistive phenomenon, but data at our disposal suggest the anode (positive pole) is probably involved.
The data as a whole suggest thus that the symmetric perovskite based cell, LSGF/LSGM/LSGF, is promising as reversible SOFC operating at intermediate temperature.

Conflicts of interest

There are no conflicts to declare.

References

[1] M.A. Laguna-Bercero, Recent advances in high temperature electrolysis using solid oxide fuel cells: A review J. Pow. Sour. 2012, 203:4-16. DOI: 10.1016/j.jpowsour.2011.12.019.
[2] T, Mori, R. Wepf, S. P. Jiang, Future prospects for the design of 'state-of-the-art' solid oxide fuel cells J. Phys. Energy, 2020, 2:031001. DOI: 10.1088/2515-7655/ab8f05
[3] S. D. Priya, A. I. Selvakumar, A. S. Nesaraj Overview on Ceramic and Nanostructured Materials for Solid Oxide Fuel Cells (SOFCs) Working at Different Temperatures J. Electrochem. Sci. Technol., 2020, 11: 99-116. DOI: 10.33961/jecst.2019.00612
[4]C. Wunderlich, Technology Readiness of SOFc Stacks – A Review, in Ceramics for Energy Conversion, Storage, and Distribution Systems: Ceramic Transactions, Volume 255, 2016, John Wiley & Sons, Inc. DOI: 10.1002/9781119234531
[5] M. B. Mogensen, M. Chen, H. L. Frandsen, C. Graves, J. B. Hansen, K. V. Hansen, A. Hauch, T. Jacobsen, S. H. Jensen, T. L. Skafte and X. Sun, Reversible solid-oxide cells for clean and sustainable energy Clean Energy, 2019, 3:175-207. DOI: 10.1093/ce/zkz023
[6] P. Di Giorgio, U. Desideri, Potential of reversible solid oxide cells as electricity storage system Energies, 2016, 9:662. DOI: 10.3390/en9080662
[7] D. Ferrero, A. Lanzini, P. Leone and M. Santarelli, Reversible operation of solid oxide cells under electrolysis and fuel cell modes: Experimental study and model validation Chem. Eng. J. 2015; 274: 143–155. DOI: 10.1016/j.cej.2015.03.096
[8] C. H. Wendel, P. Kazempoor and R. J. Braun, Novel electrical energy storage system based on reversible solid oxide cells: System design and operating conditions J. Power Sources, 2015; 276:133–144. DOI: 10.1016/j.jpowsour.2014.10.205
[9] C. H. Wendel, Z. Gao, S. A. Barnett and R. J. Braun, Modeling and experimental performance of an intermediate temperature reversible solid oxide cell for high-efficiency, distributed-scale electrical energy storage J. Power Sources, 2015; 283:329–342. DOI: 10.1016/j.jpowsour.2015.02.113
[10] C. H. Wendel, P. Kazempoor and R. J. Braun, A thermodynamic approach for selecting operating conditions in the design of reversible solid oxide cell energy systems J. Power Sources, 2016; 301:93–104. DOI: 10.1016/j.jpowsour.2015.09.093
[11] C. H. Wendel and R. J. Braun, Design and techno-economic analysis of high efficiency reversible solid oxide cell systems for distributed energy storage Appl. Energy, 2016; 172:118–131. DOI: 10.1016/j.apenergy.2016.03.054
[12] P. Kazempoor and R. J. Braun, Model validation and performance analysis of regenerative solid oxide cells for energy storage applications: Reversible operation Int. J. Hydrogen Energy, 2014; 39:5955–5971. DOI: 10.1016/j.ijhydene.2014.01.186
[13] M. Frank, R. Deja, R. Peters, L. Blum and D. Stolten, Bypassing renewable variability with a reversible solid oxide cell plant Appl. Energy, 2018; 217:101–112. DOI: 10.1016/j.apenergy.2018.02.115
[14] J. Mermelstein and O. Posdziech, Development and Demonstration of a Novel Reversible SOFC System for Utility and Micro Grid Energy Storage Fuel Cells, 2017; 17:562–570. DOI: 10.1002/fuce.201600185
[15] G. Vialetto M. Noro, P. Colbertaldo, M. Rokni, Enhancement of energy generation efficiency in industrial facilities by SOFC-SOEC systems with additional hydrogen production Int. J. Hydrogen Energy 2019; 44:9608-9620. DOI: 10.1016/j.ijhydene.2018.08.145;
[16] M. Lototskyy, S.N. Nyamsi, S. Pasupathi, W. Waernhus, A. Vik, C. Ilea, V. Yartys, A concept of combined cooling, heating and power system utilising solar power and based on reversible solid oxide fuel cell and metal hydrides Int. J. Hydrogen Energy (2008) 43:18650-18663. DOI: 10.1016/j.ijhydene.2018.05.075
[17] D. M. Bastidas, S. Tao and J. T. S. Irvine, A symmetrical solid state fuel cell demonstrating redox stable perovskite electrodes J. Mater. Chem., 2006; 16:1603. DOI: 10.1039/b600532b
[18] L. Barelli, G. Bidini, G. Cinti, A. Ottaviano Study of SOFC-SOE transition on a RSOFC stack Int. J. Hydrogen Energy, 2017, 42:26037-26047. DOI: 10.1016/j.ijhydene.2017.08.159
[19] M. Hauck, S. Herrmann, H. Spliethoff, Simulation of a reversible SOFC with Aspen Plus Int. J. Hydrogen Energy, 2017, 42:10329-10340. DOI: 10.1016/j.ijhydene.2017.01.189;
[20] A. Muramoto, Y. Kikuchi, Y. Tachikawa, SM Lyth, Y. Shiratori, S. Taniguchi, K. Sasaki High-pressure C-H-O diagrams: fuel composition, carbon deposition and open circuit voltage of pressurized SOFCs Int. J. Hydrogen Energy, 2017, 42:30769-30786. DOI: 10.1016/j.ijhydene.2017.10.122

[21] T. Daio, P. Mitra, S.M. Lyth, K. Sasaki, Atomic-resolution analysis of degradation phenomena in SOFCS: a case study of SO_3 poisoning in LSM cathodes Int. J. Hydrogen Energy, 2016, 41:12214-12221. DOI: 10.1016/j.ijhydene.2016.05.216
[22] J. Shen, G. Yang, Z. Zhang, M. O. Tadé, W. Zhou and Z. Shao, Improved performance of a symmetrical solid oxide fuel cell by swapping the roles of doped ceria and $La_{0.6}Sr_{1.4}MnO_{4+\delta}$ in the electrode J. Power Sources, 2017; 342:644–651. DOI: 10.1016/j.jpowsour.2016.12.109
[23] J. C. Ruiz-Morales, D. Marrero-López, J. Canales-Vázquez and J. T. S. Irvine, Symmetric and reversible solid oxidefuel cells RSC Adv., 2011; 1:1403 DOI: 10.1039/C1RA00284H
[24] L.Z. Bian, L.J. Wang, C.C Duan, C.K. Cai, X.W. Song, S.I. An Co-free $La_{0.6}Sr_{0.4}Fe_{0.9}Nb_{0.1}O_{3\text{-delta}}$ symmetric electrode for hydrogen and carbon monoxide solid oxide fuel cell Int. J. Hydrogen Energy, 2019; 44:32210-32218. DOI: 10.1016/j.ijhydene.2019.10.090;
[25] H. Zhang, W. Liu, HY.H. Wang, J.X. Wang, J. Yang, T.X. Liang, C.L. Yin, CL, B. Chi, L.C. Jia, W.B. Guan, Performance and long-term durability of direct-methane flat-tube solid oxide fuel cells with symmetric double-sided cathodes Int. J. Hydrogen Energy, 2019, 44:28947-28957 DOI: 10.1016/j.ijhydene.2019.09.126
[26] A. Bedon, M. Rieu, J.-P. Viricelle and A. Glisenti, Rational Development of IT-SOFC Electrodes Based on the Nanofunctionalization of La 0.6 Sr 0.4 Ga 0.3 Fe 0.7 O 3 with Oxides. PART 1: Cathodes by Means of Iron Oxide ACS Appl. Energy Mater., 2018; 1:6840–6850. DOI: 10.1021/acsaem.8b01124
[27] T. Ishihara, in AIP Conference Proceedings, 2017, vol. 1877, p. 020001
[28] C.-C. Chao, C.-M. Hsu, Y. Cui and F. B. Prinz, Improved Solid Oxide Fuel Cell Performance with Nanostructured Electrolytes ACS Nano, 2011; 5:5692–5696. DOI: 10.1021/nn201354p
[29] T. Ishihara, N. M. Sammes and O. Yamamoto, in High Temperature and Solid Oxide Fuel Cells, Elsevier, 2003, pp. 83–117
[30] C. Yang, Z. Yang, C. Jin, M. Liu and F. Chen, High performance solid oxide electrolysis cells using $Pr_{0.8}Sr_{1.2}(Co,Fe)_{0.8}Nb_{0.2}O_{4+\delta}$–Co–Fe alloy hydrogen electrodes Int. J. Hydrogen Energy, 2013; 38:11202–11208. DOI: 10.1016/j.ijhydene.2013.06.086
[31] T. H. Shin, J.-H. Myung, M. Verbraeken, G. Kim and J. T. S. Irvine, Oxydeficient layered double perovskite as an active cathode for CO_2 electrolysis using a solid oxide conductor Faraday Discuss., 2015; 182:227–239. DOI: 10.1039/c5fd00025d
[32] X.. Zhang, S. Ohara, R. Maric, H. Okawa, T. Fukui, H. Yoshida, T. Inagaki and K. Miura, Interface reactions in the NiO–SDC–LSGM system Solid State Ionics, 2000; 133:153–160. DOI: 10.1016/S0167-2738(00)00744-X
[33] A. T. Duong and D. R. Mumm, On the interaction of SSC and LSGM in composite SOFC electrodes J. Power Sources, 2013; 241:281–287.. DOI: 10.1016/j.jpowsour.2013.04.046
[34] K. Chen and S. P. Jiang, J. Electrochem. Soc., Review—Materials Degradation of Solid Oxide Electrolysis Cells Fuel Cells, Electrolyzers, and Energy Conversion 2016; 163:F3070–F3083 DOI:10.1149/2.0101611jes
[35] X. Yue, J.T.S. Irvine, Modification of LSCM–GDC cathodes to enhance performance for high temperature CO2 electrolysis using solid oxide electrolysis cells (SOECs), J: Mater. Chem. A, 2017, 5, 7081-7090. DOI: 10.1039/C6TA09421J
[36] A. Bedon, M. M. Natile and A. Glisenti, On the synthesis and stability of $La_{0.6}Sr_{0.4}Ga_{0.3}Fe_{0.7}O_3$ J. Eur. Ceram. Soc., 2017; 37:1049–1058. DOI: 10.1016/j.jeurceramsoc.2016.10.017
[37] K. Huang, J.-H. Wan and J. B. Goodenough, Increasing Power Density of LSGM-Based Solid Oxide Fuel Cells Using New Anode Materials J. Electrochem. Soc., 2001; 148:A788-A794 DOI:10.1149/1.137828
[38] R. Polini, A. Falsetti and E. Traversa, Sol–gel synthesis and characterization of Co-doped LSGM perovskites J. Eur. Ceram. Soc., 2005; 25:2593–2598. DOI: 10.1016/j.jeurceramsoc.2005.03.108
[39] P.-M. Geffroy, J. Fouletier, N. Richet and T. Chartier, Rational selection of MIEC materials in energy production processes Chem. Eng. Sci., 2013;87:408–433. DOI: 10.1016/j.ces.2012.10.027
[40] K. Bin Yoo and G. M. Choi, Performance of La-doped strontium titanate (LST) anode on $LaGaO_3$-based SOFC. Solid State Ionics, 2009;180:867–871. DOI: 10.1016/j.ssi.2009.02.013
[41] B. Philippeau, F. Mauvy, C. Mazataud, S. Fourcade and J.-C. Grenier, Comparative study of electrochemical properties of mixed conducting $Ln_2NiO_{4+\delta}$ (Ln = La, Pr and Nd) and $La_{0.6}Sr_{0.4}Fe_{0.8}Co_{0.2}O_{3-\delta}$ as SOFC cathodes associated to $Ce_{0.9}Gd_{0.1}O_{2-\delta}$, $La_{0.8}Sr_{0.2}Ga_{0.8}Mg_{0.2}O_{3-\delta}$ and $La_9Sr_1Si_6O_{26.5}$ electrolytes Solid State Ionics, 2013; 249–250:17–25. DOI: 10.1016/j.ssi.2013.06.009
[42] N. Grunbaum, L. Dessemond, J. Fouletier, F. Prado, L. Mogni and A. Caneiro, Rate limiting steps of the porous $La_{0.6}Sr_{0.4}Co_{0.8}Fe_{0.2}O_{3-\delta}$ electrode material Solid State Ionics, 2009; 180:1448–1452. DOI: 10.1016/j.ssi.2009.09.005
[43] T. Zhu, D. E. Fowler, K. R. Poeppelmeier, M. Han and S. A. Barnett, Hydrogen Oxidation Mechanisms on Perovskite Solid Oxide Fuel Cell Anodes J. Electrochem. Soc., 2016; 163:F952–F961 DOI:10.1149/2.1321608jes
[44] Q. X. Fu, F. Tietz and D. Stöver, $La_{0.4}Sr_{0.6}Ti_{1-x}Mn_xO_{3\text{-delta}}$ perovskite as anode materials for solid oxide fuel cells J. Electrochem. Soc., 2006; 153:D74. DOI: 10.1149/1.2170585
[45] K. Hosoi, H. Hagiwara, S. Ida and T. Ishihara, J. Phys. Chem. C, 2016; 120:16110–16117. DOI: 10.1021/acs.jpcc.5b12755
[46] X. Yang and J. T. S. Irvine, $(La_{0.75}Sr_{0.25})_{0.95}Mn_{0.5}Cr_{0.5}O_3$ as the cathode of solid oxide electrolysis cells for high temperature hydrogen production by steam J. Mater. Chem., 2008; 18:2349. DOI: 10.1039/b800163d